Second International Conference on CFD in the Minerals and Process Industries
CSIRO, Melbourne, Australia
6-8 December 1999

A PRESSURE CORRECTION METHOD FOR CALCULATING THE FLOWS IN LOW SPEED AXIAL FANS AND COMPRESSORS

N.X. CHEN Y.J. XU W.G. HUANG

Institute of Engineering Thermophysics, CAS, P.O. Box 2706, Beijing 100080, China

J.J.J. CHEN X.D. CHEN

Dept. of Chemical and Materials Engineering, The Auckland University, Auckland, New Zealand

Z.D. CHEN

Advanced Thermo-Fluids, Technologies Laboratory, CSIRO Building, Construction and Engineering, P.O. Box 56, Highett, Victoria 3190, Australia

ABSTRACT

In the present paper a computational method based on a pressure correction technique and coupled with a two-equation turbulence model is presented for the three-dimensional viscous flow computation in low speed axial fans and compressors. A wall function is also used for reducing the number of meshes. The time-averaged Navier-Stokes equations, written in a generalized form, are expressed by curvilinear coordinate system to fit the complex configuration of blade channel. The mesh applied here is a general structured body-fitted grid system where the curvilinear coordinate lines are coincided with the boundaries of the flow domain. In this method the governing equations are still expressed by the Cartesian coordinate system, and a coordinate transformation technique is used. The contravariant velocity components are also used only for simplifying the expression. Their directions are agreed with the curvilinear coordinate lines. The predicted results are presented here in the paper and compared with experiment.

Keywords: CFD, axial fans and compressor, aerodynamics of turbomachinery, 3-D turbulent flow

INTRODUCTION

Axial fans and compressors currently find a wide range of applications in chemical, minerals and process industries due to their ability to achieve high efficiency and high flow rate. Designs of modern high performance axial compressors trend continue to increase total pressure ratio and efficiency, and reduce weight. Lacking the knowledge of the flow structure inside turbomachine is one of the main obstacles for its development. The rapid progress of computer science and technology and computational technique enable us to apply CFD for predicting the flow phenomena in the design step of these machines.

The objective of this paper is to present a method for calculating the 3-D flow and to compare the results with experiment. As an example, a low speed single rotor compressor was calculated. The calculated results were compared with the experimental data obtained by the Beijing University of Aeronautics and Astronautics (Jiang et al., 1992).

The current method in turbomachinery computations is based on the Reynolds-averaged Navier-Stokes equations with a two-equation turbulence model. The pressure correction method proposed by Launder, Spalding (1974) and Patankar (1980). It with great success initially is used for low speed and incompressible flows and later for compressible flow as Hah (1980), Rhia et al (1984), Tourlidakis et al (1993).

The present pressure correction method is derived from authors' previous method (Chen and Xu, 1990, 1991). The difference of the present method from the previous method is only the use of the velocity components of Cartesian coordinates as the variables to be solved. The present method is used to calculate the flow in the single rotor test compressor. The in-depth validation includes span-height distributions of pitch-wisely mass-averaged parameters, contours of parameters on different coordinate surfaces. It is shown that calculation results mostly are closed to the measured data.

NOMENCLATURE

C_1, C_2, C_μ	empirical coefficients (see Eqs.(7),(11))
c_p	specific heat at constant pressure
$\vec{e}^{\,j}, \vec{e}_j$	base vector and reciprocal base vector
$\vec{F}_{vis}, f_x, f_y, f_z$	viscous force vector and its *x-, y-* and *z*-components
f^j, f_j	contravariant and covariant components of viscous force vector
G	production rate of turbulent kinetic energy (see Eq.(12))
$g,\ g^{ij}, g_{ij}$	metric tensors
$g, h, i, j, k, l, m, n, ...$	indices
$I = c_p T + 0.5(\vec{W}\cdot\vec{W} + (\vec{\Omega}\times\vec{R})(\vec{\Omega}\times\vec{R}))$	rothalpy
$\vec{i}_x, \vec{i}_y, \vec{i}_z$	unit vectors along *x-*,*y-* and *z*-coordinates
J	Jacobian , $J = \sqrt{g}$
$P,\ P_{10}$	total pressure and inlet total pressure
	total pressure at inlet
p	static pressure

$\mathrm{Pr}_l, \mathrm{Pr}_t$	laminar and turbulent numbers, respectively
R	gas constant
$\vec{R}, r^j, r_j$	radius vector and its contravariant and covariant components
R_1, R_2	radius at inlet and outlet (see Eq.(19))
S_Φ	source term (see Eq.(8-11))
T	absolute temperature
$U_{tip} = \Omega R_{tip}$	rotating speed at tip
$\vec{V}, V_{t1}, V_{t2}$	absolute velocity vector and its inlet and outlet circumferential velocity
$\vec{W}, W^j, W_j, w^j, w_j$	relative velocity vector and its physical contravariant, physical covariant, contravariant and covariant components
W_x, W_y, W_z or w_x, w_y, w_z	x-,y- and z-components of relative velocity vector
β	relative flow angle
E_{ij}	component of viscous strain tensor $\vec{\vec{\mathrm{E}}}$
ε	dissipation rate of turbulent energy
$\varepsilon^{jki}, \varepsilon_{jki}$	Eddington tensors
$\Phi = 1, w_x, w_y, w_z, I, \kappa, \varepsilon$	one of the variables to be solved,
Φ^*	dissipation function (see Eq.(13))
ϕ	flow rate coefficient, $\phi = V_x / U_{tip}$
$\Gamma_\Phi = 0, \mu_{eff}, \mu_{eff}, \mu_{eff}, \lambda_{eff}/c_p, \mu_t/\sigma_\kappa, \mu_t/\sigma_\varepsilon$	one of the effective diffusion coefficients,
Γ_{ij}^k	Christoffel symbol
κ	turbulent kinetic energy
$\lambda_l, \lambda_t, \lambda_{eff} (or \lambda)$	laminar, turbulent and effective coefficient of thermal conductivity
$\mu_l, \mu_t, \mu_{eff} (or \mu)$	laminar, turbulent and effective dynamic viscosity
$\vec{\Omega}, \omega^j, \omega_j$	angular velocity vector, its contra-variant and covariant components
Π_{ij}	component of viscous stress tensor $\vec{\vec{\Pi}}$
ρ	density
ς_p	pressure loss coefficient
$(\,)\big\vert_j$	covariant derivative of $(\,)$

NUMERICAL METHOD

Reynolds equations in tensor form

On the basis of governing equations expressed by non-orthogonal curvilinear coordinate system a pressure-correction method for 3-D turbulent flow in turbomachinery is present in the present paper. The two-equation turbulent model and a wall function are used.

The Reynolds averaged Navier-Stokes equations can be written in tensor form as follows:

1. Continuity equation:

$$\partial\rho/\partial t + (\rho w^j)\big|_j = 0 \tag{1}$$

2. Momentum equation

in $\vec{e}_j$ - *direction*:

$$\rho\partial w^j/\partial t + \rho w^i w^j\big|_i - \rho\Omega^2 r^j + 2\rho\omega_k w_i \varepsilon^{jki} = g^{im} g^{jl} (\Pi_{ml}\big|_i) - g^{jl} p\big|_l \tag{2}$$

in $\vec{e}^{\,j}$ - *direction*:

$$\rho\partial w_j/\partial t + \rho w^i w_j\big|_i - \rho\Omega^2 r_j + 2\rho\omega^k w^i \varepsilon_{jki} = g^{im}(\Pi_{ml}\big|_i) - p\big|_i \tag{3}$$

3. Energy equation:

$$\rho\partial I/\partial t + \rho w^i I\big|_i = \partial p/\partial t + (g^{im}\lambda T\big|_m)\big|_i + g^{im} w^j \Pi_{mj}\big|_i + g^{im} g^{lj} \Pi_{mj} \mathrm{E}_{il} \tag{4}$$

The viscous stress is the function of velocity as:

$$\Pi_{ij} = \mu E_{ij} = \mu\left(\frac{\partial w_j}{\partial x^i} + \frac{\partial w_i}{\partial x^j} - 2w_k\Gamma_{ij}^k - \frac{2}{3} g_{ij} div\vec{W}\right) \tag{5}$$

There is a summation over all repeated indices. The rotation is along the x - coordinate axis. The relationship between relative and absolute velocity vectors is $\vec{W} = \vec{V} - \vec{\Omega}\times\vec{R}$. The first terms of the right-hand side of the momentum equations, Eqs.(2) and (3), are the contravariant and covariant components of viscous force vector $\vec{F}_{vis}$, i.e. $(f_{vis})^j$ and $(f_{vis})_j$. The second term on the right-hand side of the energy equation is heat-transfer term which represents the heat added from outside to the present control volume of the fluid per unit time. The third and forth terms are the rates of work done by viscous stresses consist of two parts. They are: the first one is caused by the change of the viscous forces, that is shown in the third term on the right-hand side of the energy equation, which is the dot product of relative velocity and viscous force vectors $\vec{F}_{vis}\cdot\vec{W}$. The second part is the forth term caused by the deformation of the fluid on which the viscous stresses act. We call it dissipation function Φ^*. These equations are conveniently and easily used for the computational domain with complex configuration. In these cases the unknown variables of the momentum equation to be solved are the contravariant and covariant, respectively.

Governing equations expressed by Cartesian coordinate system

In the present paper the x-, y- and z-components of the momentum equation are used, and then the variables of the momentum equation are w_x, w_y and w_z. The above-mentioned governing equations for steady flow coupled with $\kappa-\varepsilon$ model expressed by the Cartesian coordinate system can be written in a generalized form as follow:

$$\frac{\partial(\rho\Phi)}{\partial t} + \frac{\partial(\rho w_x\Phi)}{\partial x} + \frac{\partial(\rho w_y\Phi)}{\partial y} + \frac{\partial(\rho w_z\Phi)}{\partial z}$$

$$\frac{\partial}{\partial x}(\Gamma_\Phi \frac{\partial \Phi}{\partial x})+\frac{\partial}{\partial y}(\Gamma_\Phi \frac{\partial \Phi}{\partial y})+\frac{\partial}{\partial z}(\Gamma_\Phi \frac{\partial \Phi}{\partial z})+S_\Phi \quad (6)$$

where: Φ denotes the variable to be solved, $\Phi = 1, w_x, w_y, w_z, I, \kappa, \varepsilon$; Γ_Φ is the effective diffusion coefficient and S_Φ is the source term. They are defined as: $\Gamma_\Phi = 0, \mu_{eff}, \mu_{eff}, \mu_{eff}, \lambda_{eff}/c_p, \mu_t/\sigma_\kappa, \mu_t/\sigma_\varepsilon$ and $S_\Phi = 0, S_{w_x}, S_{w_y}, S_{w_z}, S_I, S_\kappa, S_\varepsilon$ for continuity equation, three components of momentum equation, energy equation, $\kappa-$ and $\varepsilon-$ equations, respectively. The empirical coefficients are $\sigma_\kappa = 1.0$ and $\sigma_\varepsilon = 1.3$. The effective dynamic viscosity μ_{eff} and effective conductivity ë $_{\text{eff}}$ can be determined as: $\mu_{eff} = \mu_t + \mu_t$ and $\lambda_{eff} = \lambda_l + \lambda_t = c_p(\mu_l/\mathrm{Pr}_l + \mu_t/\mathrm{Pr}_t)$. Later we will denote μ_{eff}, λ_{eff} by μ, λ, respectively. The turbulent dynamic viscosity is calculated as follows:

$$\mu_t = C_\mu \rho\ \kappa^2/\varepsilon \quad (7)$$

$$\begin{aligned} S_{w_x} &= \partial(\mu\partial w_x/\partial x)/\partial x + \partial(\mu\partial w_y/\partial x)/\partial y \\ &+ \partial(\mu\partial w_z/\partial x)/\partial z - (2/3)\partial(\mu div\vec{W})/\partial x - \partial p/\partial x \end{aligned} \quad (8a)$$

$$\begin{aligned} S_{w_y} &= \partial(\mu\partial w_x/\partial y)/\partial x + \partial(\mu\partial w_y/\partial y)/\partial y \\ &+ \partial(\mu\partial w_z/\partial y)/\partial z - (2/3)\partial(\mu div\vec{W})/\partial y - \partial p/\partial y \\ &+ \rho\Omega^2 y + 2\rho\Omega w_z \end{aligned} \quad (8b)$$

$$\begin{aligned} S_{w_3} &= \partial(\mu\partial w_x/\partial z)/\partial x + \partial(\mu\partial w_y/\partial z)/\partial y \\ &+ \partial(\mu\partial w_z/\partial z)/\partial z - (2/3)\partial(\mu div\vec{W})/\partial z - \partial p/\partial z \\ &+ \rho\Omega^2 z - 2\rho\Omega w_y \end{aligned} \quad (8c)$$

$$\begin{aligned} S_I = &-0.5\partial\{(\lambda/c_p)[\partial(\vec{W}\cdot\vec{W})/\partial x]\}/\partial x - \\ &0.5\partial\{(\lambda/c_p)[\partial(\vec{W}\cdot\vec{W})/\partial y]\}/\partial y \\ &- 0.5\partial\{(\lambda/c_p)[\partial(\vec{W}\cdot\vec{W})/\partial z]\}/\partial z + \Phi^* \\ &+ \rho(f_x w_x + f_y w_y + f_z w_z) \end{aligned} \quad (9)$$

$$S_\kappa = \mu_t G - \rho\varepsilon \quad (10)$$

$$S_\varepsilon = C_1\mu_t(\varepsilon/\kappa)G - C_2\rho\varepsilon^2/\kappa \quad (11)$$

where $G, \Phi^*, \vec{F}_{vis}$ are the production rate of turbulence kinetic energy, dissipation rate and viscous force, respectively. They are calculated as follows:

$$\begin{aligned} G = &2[(\partial w_x/\partial x)^2 + (\partial w_y/\partial y)^2 + (\partial w_z/\partial z)^2] \\ &+ [(\partial w_x/\partial y + \partial w_y/\partial x)^2 \\ &+ (\partial w_y/\partial z + \partial w_z/\partial y)^2 + (\partial w_z/\partial x + \partial w_x/\partial z)^2] \end{aligned} \quad (12)$$

$$\begin{aligned} \Phi^* = &2\mu[(\partial w_x/\partial x)^2 + (\partial w_y/\partial y)^2 + (\partial w_z/\partial z)^2] \\ &+ \mu[(\partial w_x/\partial y + \partial w_y/\partial x)^2 + \\ &(\partial w_y/\partial z + \partial w_z/\partial y)^2 + (\partial w_x/\partial z + \partial w_z/\partial x)^2] \end{aligned} \quad (13)$$

$$\vec{F}_{vis} = f_x\vec{i}_x + f_y\vec{i}_y + f_z\vec{i}_z \quad (14)$$

$$\begin{aligned} f_x = &\{\partial(2\mu\partial w_x/\partial x - (2/3)\mu div\vec{W})/\partial x \\ &+ \partial[\mu(\partial w_x/\partial y + \partial w_y/\partial x)]/\partial y \\ &+ \partial[\mu(\partial w_x/\partial z + \partial w_z/\partial x)]/\partial z\}/\rho \end{aligned} \quad (15a)$$

$$\begin{aligned} f_y = &\{\partial(2\mu\partial w_y/\partial y - (2/3)\mu div\vec{W})/\partial y \\ &+ \partial[\mu(\partial w_x/\partial y + \partial w_y/\partial x)]/\partial x \\ &+ \partial[\mu(\partial w_y/\partial z + \partial w_z/\partial y)]/\partial z\}/\rho \end{aligned} \quad (15b)$$

$$\begin{aligned} f_z = &\{\partial(2\mu\partial w_z/\partial z - (2/3)\mu div\vec{W})/\partial z \\ &+ \partial[\mu(\partial w_x/\partial z + \partial w_z/\partial x)]/\partial x \\ &+ \partial[\mu(\partial w_y/\partial z + \partial w_z/\partial y)]/\partial y\}/\rho \end{aligned} \quad (15c)$$

In Equations (7) and (11) C_1, C_2, C_μ are the empirical coefficients of $\kappa-\varepsilon$ model. They are 1.47, 1.92, 0.09, respectively.

Coordinate transformation technique

The mesh employed is a general structured grid system where curvilinear coordinate lines coincide with the boundaries of the flow domain. Therefore, it is need to use the coordinate transformation technique to have a body-fitted coordinate system. Then, introducing new independent variables, $x^1 = x^1(x,y,z)$, $x^2 = x^2(x,y,z)$, $x^3 = x^3(x,y,z)$, the generalized form of the governing equations, Eq.(6), can be expressed by the body-fitted curvilinear coordinate system as follows:

$$\begin{aligned} &\frac{\partial(\rho\sqrt{g}\Phi)}{\partial t} + \frac{\partial(\rho W^1\Phi)}{\partial x^1} + \frac{\partial(\rho W^2\Phi)}{\partial x^2} + \frac{\partial(\rho W^3\Phi)}{\partial x^3} = \\ &\frac{\partial(J\Gamma_\Phi g^{11}\frac{\partial\Phi}{\partial x^1})}{\partial x^1} + \frac{\partial(J\Gamma_\Phi g^{22}\frac{\partial\Phi}{\partial x^2})}{\partial x^2} + \frac{\partial(J\Gamma_\Phi g^{33}\frac{\partial\Phi}{\partial x^3})}{\partial x^3} \\ &+ S_i'(x^1, x^2, x^3) \end{aligned} \quad (16)$$

The physical contravariant relative velocity components, W^1, W^2, W^3, are defined by:

$$\begin{aligned} W^1 &= J(w_x\partial x^1/\partial x + w_y\partial x^1/\partial y + w_z\partial x^1/\partial z), \\ W^2 &= J(w_x\partial x^2/\partial x + w_y\partial x^2/\partial y + w_z\partial x^2/\partial z), \\ W^3 &= J(w_x\partial x^3/\partial x + w_y\partial x^3/\partial y + w_z\partial x^3/\partial z) \end{aligned} \quad (17)$$

where J is Jacobian of coordinate transformation.

The source term can be written as:

$$\begin{aligned} S_i'(x^1, x^2, x^3) &= JS_\Phi \\ &+ \partial(J\Gamma_\Phi g^{12}\partial\Phi/\partial x^2)/\partial x^1 + \partial(J\Gamma_\Phi g^{13}\partial\Phi/\partial x^3)/\partial x^1 \\ &+ \partial(J\Gamma_\Phi g^{21}\partial\Phi/\partial x^3)/\partial x^2 + \partial(J\Gamma_\Phi g^{23}\partial\Phi/\partial x^3)/\partial x^2 \\ &+ \partial(J\Gamma_\Phi g^{31}\partial\Phi/\partial x^1)/\partial x^3 + \partial(J\Gamma_\Phi g^{32}\partial\Phi/\partial x^2)/\partial x^3 \end{aligned} \quad (18)$$

Solution procedure

The discretized algebraic equations of generalized Eq.(16) are solved by using the pressure correction method. A central volume approximation is used for all diffusion terms, and an up-winding scheme is used for convection

terms. The difference equations for the pressure correction, the energy, the turbulent kinetic energy and dissipation rate can be written in a generalized version. The above discretized algebraic equations are solved by successive iterations with the linear relaxation method. Since the solution procedure has been given in many literatures, we would not go through it.

RESULTS

As a calculated example a single rotor test compressor of BUAA is used. It is consisted from 17 twisted blades mounted on the hub. The tip and hub diameters are 1000 mm and 600 mm, respectively. The tip clearance is about one mm. The design rotating speed of the rotor is 1200 rpm. Some of the calculated results are compared with experimental results. A body-fitted non-uniform H-type grid system with the grid number of 30x98x35 is applied for the calculation (see Figure 1). It is automatically generated by the GRID_TURBO3 code proposed by the authors. From the figure it is clearly seem that near wall, blade surfaces, inlet and outlet boundaries finer meshes are used.

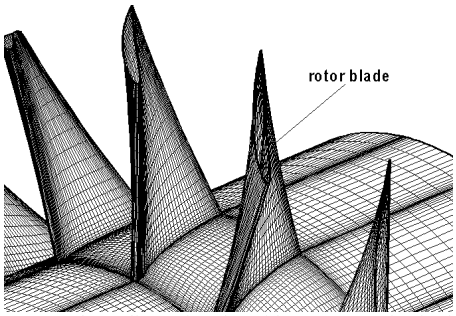

Figure 1: Three-dimensional grid system of single rotor compressor

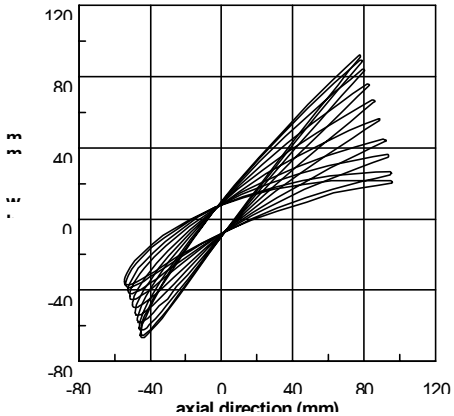

Figure 2: Blade profiles of different span height radius

In Figure 2 the blade profiles at different radius are shown. Fig.3 presents the computational domain. Station 1 and station 4 are inlet and outlet of the computational domain, respectively. Station 3 is the measured plane located at 20 mm from the trailing edge of the rotor blade row. The design condition is at the point which flow rate coefficient equals 0.58 approximately. The calculated pressure rise is a little bit lower than the measured. The following calculated results are compared with experiment only for the design condition.

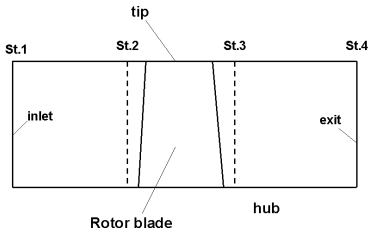

Figure 3: Computational domain

In Figure 4 the grid point length of x-, circumferential and span-wise directions are shown. From this figure it is seen there are very smooth coordinate lines. Near inlet, outlet boundaries and the mid-blade-channel the meshes are coarse, and near blade surfaces the meshes are finer.

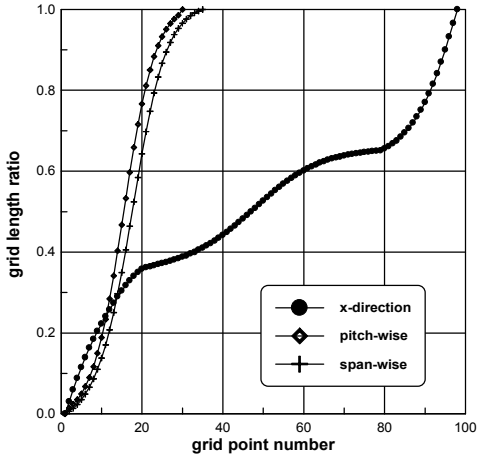

Figure 4: Relative length of grid points for three directions

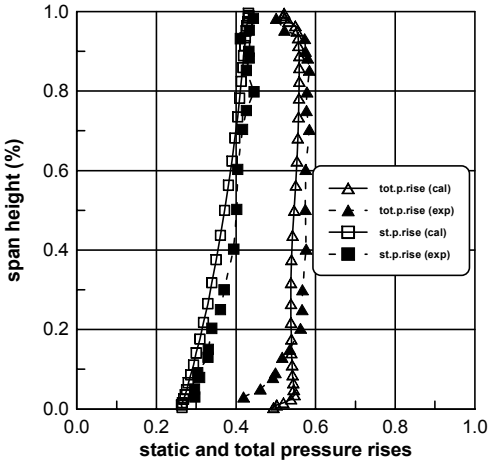

Figure 5: Comparison between calculated and measured distributions of static and total pressure rises along span height

Span height distributions of pitch-wisely mass-average parameters

All averaged parameters at below are obtained by the pitch-wisely mass-averaging procedure. The span-wise distributions of static and total pressure rises calculated and measured are plotted in figure 5. The calculated results are lower than the measured. In Figure 6 the comparison between the calculated and measured data of absolute velocity components V_x / U_{tip}, V_t / U_{tip}, V_r / U_{tip} is illustrated. Figure 7 shows the span-wise distributions of calculated and measured flow rate coefficient ϕ and pressure loss coefficients ς_P. The latter is defined as follows:

$$\varsigma_P = \frac{(\Omega R_2 V_{t2} - \Omega R_1 V_{t1}) - (P - P_{10}) / \rho}{U_{tip} / 2} \qquad (19)$$

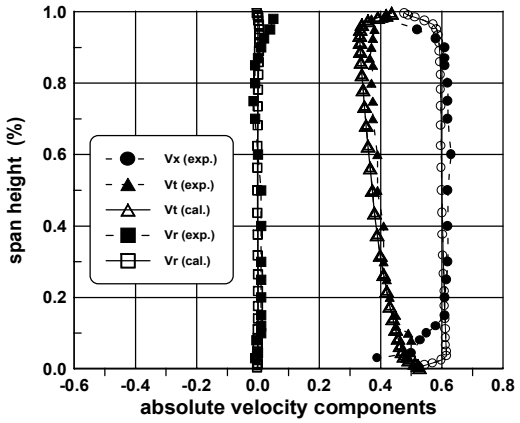

Figure 6: Comparison between calculated and measured absolute velocity components along span height at exit from rotor(st.3)

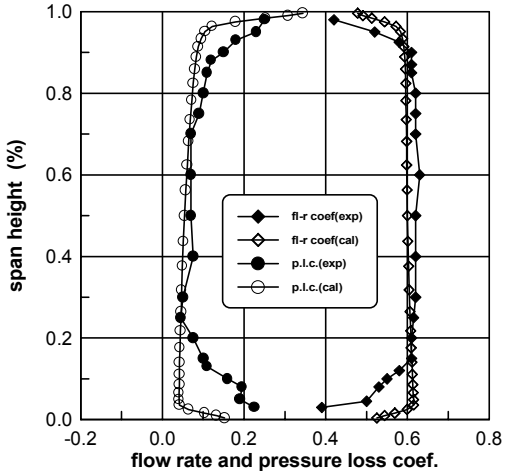

Figure 7: Comparison between calculated and measured distributions of flow rate and pressure loss coefficients

As shown in the figure at center of the span the calculated data are very closed to the measured data. The relative flow angle is one of the important design parameters. In Figure 8 the comparison between its calculated and measured distributions is plotted.

From above figures it is seen that the results in the region near mid-span the calculated by the present method are agreed with experiment very well. All results at hub and tip differ from the experiment. This is because in the present paper the tip and hub clearance effects have not been taken into account. Due to the inadequate accuracy of manufacturing there exists a gap between the hub surface and the rotor blades. From experience it is seen with increasing tip clearance the pressure loss coefficient is increased. The effect of the tip clearance on the flow feathers for the present single rotor compressor will be discussed in the another paper.

Parameters contours on the surfaces of revolution and the constant-x-coordinate surfaces

In this suction we will show the calculated results on the S_1- and S_3-coordinate surfaces, i.e. on the surfaces of revolution and the constant-x-coordinate surfaces, respectively, and their comparison with the measured data. Unfortunately there are no measured data of pressure contours on the surface of revolution. We will show them only for illustration. In Figure 9 the static pressure contours on the surfaces of revolution at hub-, mid- and tip-span heights.

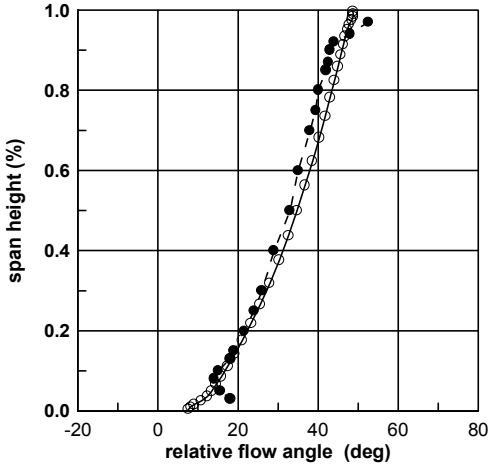

Figure 8: Comparison between calculated and measured relative flow angle distributions along span height

For the constant-*x*-coordinate surfaces the calculated contours are shown and compared with experiment at the exit from the rotor (st.3). Station No.3 is the measuring plane located at 20 mm out of the trailing edge of the rotor blade row. At this plane all the velocity, pressure contours were calculated and compared with experiment. In this paper we could not show all of them due to the limitation of pages. Due to the importance of the relative flow angle their calculated contours are plotted in Figure 10. The calculated data are as the lower figure and the measured data are also plotted in the upper one. They are closed each to other.

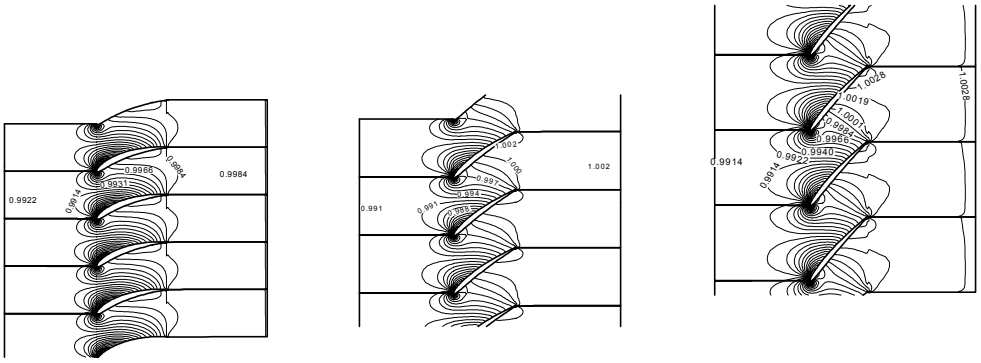

Figure 9: Static pressure contours on the surfaces of revolution at tip-(right), mid-(central) and hub-(right)span heights

CONCLUSIONS

In the present paper a pressure correction method is presented. It can be used to calculate the flow field in fans and compressors. As an example the 3D turbulent flow in a test low-speed axial single rotor compressor was calculated. At beginning of the paper the basic equations of the turbulent flow in turbomachinery are given. A coordinate transformation technique is used in this paper. The equations are written in a generalized form for adapting the body-fitted coordinate system. The in-depth validation includes span-height distributions of pitch-wisely mass-averaged parameters, contours of parameters on different coordinate surfaces. For comparison the calculated results are plotted together with measured data. It is shown that the calculation results are closed to the experiment. Due to tip clearance effect that has not been taken into account there exists some discrepancy in the near wall region. In the future studies of appropriate consideration of the tip clearance effect will be carried out. The present work has proved that the method can be used for studying the flow phenomena in turbomachinery.

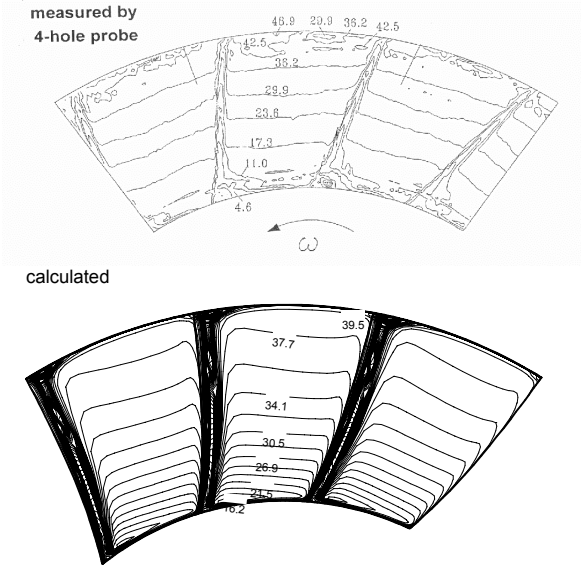

Figure 10: Contours of relative flow angle at st.3 (rotor exit)

ACKNOWLEDGEMENTS

The authors are grateful to Professor Jiang, H.K. and Dr. Ma, H.W. for their experimental results. We would like to acknowledge China National Key Projects, China National Natural Science Foundation and the New Zealand Foundation for Research Science and Technology for their partial support to this work.

REFERENCES

CHEN, Naixing and Xu, Yanji, (1990) Numerical Computation of 3-D Turbulent Flow in Turbine Cascade, Chinese Sciences Bulletin, Vol. 35, No. 14.

CHEN, Naixing and Xu, Yanji, (1991) Numerical Solution of 2D and 3D Turbulent Internal Flow Problems, Int. J. Of Numerical Methods in Fluid, Vol. 13, No. 2.

HAH, C., (1984) A Navier-Stokes Analysis of Three-Dimensional Flow Inside Turbine Blade Row at Design and Off-design Conditions, J. Eng. Gas Turbine Power, Vol. 106, pp. 421-429.

JIANG, H. C., Li, Yu. C., Zhang, H., Xiong, Z., Xu, L. P. and Chen, M. Z., (1992) A Large Scale Axial Compressor Test Rig and Dynamic Measuring Technique for Studying Internal Flow Phenomena Inside the Rotor, Journal of Aerospace Power, Vol. 7, No. 1, pp. 1-8.

LAUNDER, B. E. and SPALDING, D. B., (1974) The Numerical Computation of Turbulent Flows, Computational Methods In Applied Mechanical Engineering, Vol. 3, pp.269-289.

MOORE, J. and MOORE, Y. G., (1980) Calculations of Three-Dimensional Viscous Flow and Wake Development in a Centrifugal Impeller, ASME CP Performance Prediction of Centrifugal Pumps and Compressors, pp. 61-67, 1980.

PATANKAR, S. V., Numerical Transfer and Fluid Flow, McGraw Hill, New York.

RHIE, C. M. and CHOW, W. L., (1984) Numerical Study of the Turbulent Flow Past an Airfoil with Trailing Edge Separation, AIAA Journal, Vol. 21, No. 11, pp.1525-1532.

TOURLIDAKIS, A. and ELDER, R. L., (1993) Numerical Investigations of Centrifugal Compressor Flows with Tip Leakage Using a Pressure Correction Method, ASME Paper No. 93-GE-109.